

Regular Paper

Geometric Correction of Historical Maps Based on Vector Field Analysis

TAKESHI MIURA^{1,a)} KATSUBUMI TAJIMA¹

Received: May 17, 2021, Accepted: September 9, 2021

Abstract: It is well known that the following two conditions should be satisfied in the control-point based geometric correction of historical maps: (a) Conversion from a historical map into a present map is a homeomorphism and (b) The straightness of designated specific line segments is maintained. In this paper, a new method for the control-point based geometric correction of historical maps, which simultaneously satisfies both the above conditions, is proposed. The correction process is modeled as a phenomenon in a three-dimensional vector field. Each point in a historical map is connected with the corresponding point in a present map by a streamline of the field. Since a unique streamline passes through any point in the vector field having no zero-vector point, the above connection relationship becomes a homeomorphism. As a result, Condition (a) is satisfied. On the other hand, the straightness of designated line segments is maintained because streamlines intersecting with the line segments in the historical map are formed so as to necessarily intersect with the corresponding line segments in the present map. Consequently, Condition (b) is satisfied. The experimental results demonstrate the effectiveness of the proposed method.

Keywords: historical map, geometric correction, homeomorphism, straightness, vector field

1. Introduction

Historical maps are important materials as information sources about the historical landscapes of the ages when the maps were produced. In the analysis of historical maps, a technique of geometric correction is often used to overlay them on present maps [1], [2]. This makes it possible to quantitatively compare the situation of, for example, land use in a historical map with that in a present map.

The most popular method for the geometric correction of historical maps is that in which the specific points designated by users are employed as control points [1], [2], [3], [4]. Control points are the points whose locations in both the historical and present maps are already known (e.g., temples, shrines, etc.), and used as reference points to be fixed at the designated specific positions in both the maps. All the points in a historical map, including the ones other than the control points, are converted into those in a present map so as to maintain their relative positional relationship to a certain extent and at the same time satisfy the condition that the control points are fixed at the designated positions.

It is well known that there are two main groups in control-point based geometric correction methods: global and local transformations [2], [3], [4]. In global transformation methods, only one mathematical model is used to convert the coordinates of any point in a historical map into that in a present map [2], [3]. A typical example of the mathematical model is that consisting of two polynomials for two coordinates. Their coefficients are usu-

ally adjusted by the least squares method [2]. The disadvantage of global transformation is that residual errors exist in the positions of the control points in the corrected historical map [2], [3], [4]. This means that the condition required for control points is not satisfied.

In local transformation methods, on the other hand, either a historical map is cut into areas each of which has its own mathematical model for point conversion, or the position of any point is converted with its own mathematical model [2]. A typical example of the former approach is a method based on the introduction of the triangulated irregular network with a local coordinate conversion (TIN) [1], whereas that of the latter approach is the moving least squares transformation (MLS) [5]. In local transformation, no residual error appears in the positions of the control points in the corrected historical map [1], [2]. In other words, the condition required for control points is satisfied. In this paper, we focus on the group of local transformation satisfying the above condition.

In the control-point based geometric correction of historical maps, it is required that the conditions shown below are also satisfied [1], [6]:

- (a) Conversion from a historical map into a present map is a homeomorphism (i.e., one-to-one onto mapping).
- (b) The straightness of designated specific line segments (e.g., straight roads, moats, etc.) is maintained.

Condition (a) is often violated in TIN. Therefore, an additional procedure, e.g., modifying the structure of a triangulated irregular network by hand [7], is often introduced to resolve the issue. As for Condition (b), on the other hand, an attempt to satisfy this condition is seen in Ref. [6]. In this attempt, the weighted mean of the between-map displacement amounts of designated line seg-

¹ Graduate School of Engineering Science, Akita University, Akita 010-8502, Japan

^{a)} miura@mail.ee.akita-u.ac.jp

ments is used to determine the displacement amount of a point to be converted. Although the weight is given as a function of the distance between a line segment and a point to be converted, it is not a strict inverse distance weight but a monotonously decreasing function giving only a finite value. Therefore, the weight of the line segment, on which a point to be converted on the corresponding line segment in the present map exists, does not become infinite, and thereby other line segments can affect the determination of the displacement amount of the point. As a result, the converted point does not necessarily exist on the corresponding line segment. In other words, the straightness of the line segment cannot be sufficiently maintained.

In this paper, we propose a new method for the control-point based geometric correction of historical maps. This method belongs to the group of local transformation, and is developed so as to simultaneously satisfy both Conditions (a) and (b). We model the correction process as a phenomenon in a three-dimensional vector field [8]. This concept is introduced from the map-deformation method proposed for the construction of distance cartograms [9].

We arrange historical and present maps in the vector field so that any point in the historical map is connected with a point in the present map by a streamline [8] of the field. Each of the points existing on a designated line segment (hereafter, we call it ‘‘a control line segment’’) is also connected with a point on the corresponding control line segment in the present map. When no zero-vector point exists in the field, there is a unique streamline passing through any point [8]. Therefore, the above point connection becomes a one-to-one onto mapping, i.e., homeomorphism [10]. As a result, Condition (a) is satisfied. On the other hand, the straightness of control line segments is also maintained because streamlines intersecting with the control line segments in the historical map are formed so as to necessarily intersect with the corresponding control line segments in the present map. Consequently, Condition (b) is satisfied.

We conduct experiments in which simple artificial mapping models and an actual historical map are used. We compare the proposed method with the other two local-transformation methods previously proposed: TIN and MLS. The experimental results show that the proposed method can provide characteristics better than those provided by the other two methods.

The remainder of this paper is organized as follows. We describe the vector-field-analysis based geometric correction method in Section 2. We show experimental results and verify the effectiveness of the proposed method in Section 3. A conclusion is finally summarized in Section 4.

2. Geometric Correction Based on Vector Field Analysis

2.1 Advance Preparation for Geometric Correction

As already mentioned in Section 1, historical and present maps are arranged in a three-dimensional vector field. To avoid the production of a vector field with a distribution too complicated, an appropriate spatial arrangement is needed. This section describes the detail of the advance preparation to appropriately arrange both the maps.

Suppose that the set of the control points in the historical map and the corresponding points in the present map are given as follows:

$P_{Hn}(x_{Hn}, y_{Hn})$ ^{*1}: control point for the historical map

$P_{Pn}(x_{Pn}, y_{Pn})$: control point for the present map

($1 \leq n \leq N_P$, N_P : total number of control points)

where P_{Hn} is the n th control point in the historical map and P_{Pn} is the corresponding one in the present map. We also give the set of the control line segments in the historical map and the corresponding line segments in the present map as follows:

$L_{sHm}(x_{sHm}, y_{sHm})$ $L_{eHm}(x_{eHm}, y_{eHm})$: control line segment for the historical map

$L_{sPm}(x_{sPm}, y_{sPm})$ $L_{ePm}(x_{ePm}, y_{ePm})$: control line segment for the present map

($1 \leq m \leq N_L$, N_L : total number of control line segments)

where L_{sHm} and L_{eHm} are the endpoints of the m th control line segment in the historical map and L_{sPm} and L_{ePm} are the corresponding ones in the present map. The positions of the above points are represented by the following position vectors:

$$\mathbf{p}_{Hn} = [x_{Hn} \quad y_{Hn}]^T \text{ for } P_{Hn}$$

$$\mathbf{p}_{Pn} = [x_{Pn} \quad y_{Pn}]^T \text{ for } P_{Pn}$$

$$\mathbf{l}_{sHm} = [x_{sHm} \quad y_{sHm}]^T \text{ for } L_{sHm}$$

$$\mathbf{l}_{eHm} = [x_{eHm} \quad y_{eHm}]^T \text{ for } L_{eHm}$$

$$\mathbf{l}_{sPm} = [x_{sPm} \quad y_{sPm}]^T \text{ for } L_{sPm}$$

$$\mathbf{l}_{ePm} = [x_{ePm} \quad y_{ePm}]^T \text{ for } L_{ePm}$$

To eliminate the influence of direction deviation between the historical and present maps, we rotate the latter one. In the case that the present map is rotated with the angle θ , the position vector \mathbf{p}_{Pn} of the n th control point P_{Pn} is converted into $\mathbf{p}'_{Pn}(\theta)$ of the rotated point P'_{Pn} as follows:

$$\mathbf{p}'_{Pn}(\theta) = \mathbf{R}(\theta)\mathbf{p}_{Pn} \quad (1)$$

where

$$\mathbf{R}(\theta) = \begin{bmatrix} \cos \theta & -\sin \theta \\ \sin \theta & \cos \theta \end{bmatrix}$$

The angle between the line segment formed by the pair of the n_1 th and n_2 th control points in the historical map, $P_{Hn_1}P_{Hn_2}$, and the corresponding line segment in the rotated present map, $P'_{Pn_1}P'_{Pn_2}$, becomes as follows:

$$\phi_{Pn_1, n_2}(\theta) = \cos^{-1} \frac{(\mathbf{p}_{Hn_1} - \mathbf{p}_{Hn_2}) \cdot \{\mathbf{p}'_{Pn_1}(\theta) - \mathbf{p}'_{Pn_2}(\theta)\}}{\|\mathbf{p}_{Hn_1} - \mathbf{p}_{Hn_2}\| \|\mathbf{p}'_{Pn_1}(\theta) - \mathbf{p}'_{Pn_2}(\theta)\|} \quad (2)$$

As for the m th control line segment $L_{sPm}L_{ePm}$, the position vectors of the endpoints, \mathbf{l}_{sPm} and \mathbf{l}_{ePm} , are converted into $\mathbf{l}'_{sPm}(\theta)$ and $\mathbf{l}'_{ePm}(\theta)$ corresponding to the rotated line segment $L'_{sPm}L'_{ePm}$ as follows:

$$\mathbf{l}'_{sPm}(\theta) = \mathbf{R}(\theta)\mathbf{l}_{sPm} \quad (3)$$

$$\mathbf{l}'_{ePm}(\theta) = \mathbf{R}(\theta)\mathbf{l}_{ePm} \quad (4)$$

The angle between $L_{sHm}L_{eHm}$ in the historical map and $L'_{sPm}L'_{ePm}$ in the rotated present map becomes as follows:

$$\phi_{Lm}(\theta) = \cos^{-1} \frac{(\mathbf{l}_{eHm} - \mathbf{l}_{sHm}) \cdot \{\mathbf{l}'_{ePm}(\theta) - \mathbf{l}'_{sPm}(\theta)\}}{\|\mathbf{l}_{eHm} - \mathbf{l}_{sHm}\| \|\mathbf{l}'_{ePm}(\theta) - \mathbf{l}'_{sPm}(\theta)\|} \quad (5)$$

^{*1} In this paper, the symbol x is used as the coordinate of the horizontal axis, whereas y as that of the vertical axis. This symbol assignment is contrary to that in the Japanese surveying and mapping community (x : northing, y : easting) [11]. We select the above assignment in accordance with mathematical conventions.

To obtain the optimal rotation angle θ_0 giving the rotated present map whose direction is aligned to that of the historical map, we solve the following optimization problem:

Minimize $f(\theta)$

Subject to $\theta_{\min} \leq \theta \leq \theta_{\max}$

where

$$f(\theta) = \frac{f_P(\theta) + f_L(\theta)}{g_P(\theta) + g_L(\theta)}$$

$$f_P(\theta) = \sum_{n_1=1}^{N_P-1} \sum_{n_2=n_1+1}^{N_P} v_{P_{n_1, n_2}}(\theta) \phi_{P_{n_1, n_2}}(\theta)$$

$$f_L(\theta) = \sum_{m=1}^{N_L} v_{L_m}(\theta) \phi_{L_m}(\theta)$$

$$g_P(\theta) = \sum_{n_1=1}^{N_P-1} \sum_{n_2=n_1+1}^{N_P} v_{P_{n_1, n_2}}(\theta)$$

$$g_L(\theta) = \sum_{m=1}^{N_L} v_{L_m}(\theta)$$

$$v_{P_{n_1, n_2}}(\theta) = \sqrt{|\mathbf{p}_{Hn_1} - \mathbf{p}_{Hn_2}| \left| \mathbf{p}'_{P_{n_1}}(\theta) - \mathbf{p}'_{P_{n_2}}(\theta) \right|}$$

$$v_{L_m}(\theta) = \sqrt{|\mathbf{l}_{eHm} - \mathbf{l}_{sHm}| \left| \mathbf{l}'_{ePm}(\theta) - \mathbf{l}'_{sPm}(\theta) \right|}$$

and θ_{\min} and θ_{\max} are the angles giving the search interval of the rotation angle, $[\theta_{\min}, \theta_{\max}]$. The objective function $f(\theta)$ is the weighted mean of the angles each of which is that between the historical-map line segment and the corresponding present-map line segment. Each angle is weighted with the size of the corresponding line-segment pair (specifically, weighted with the geometric mean of the length of the historical-map line segment and that of the present-map line segment, i.e., $v_{P_{n_1, n_2}}(\theta)$ or $v_{L_m}(\theta)$). This is based on the fact that direction deviation given by a line-segment pair with a larger size can bring about greater map deformation. In actual calculations, we solve the above optimization problem by the golden section search method [12]^{*2} under the conditions $\theta_{\min} = -2\pi/3$ and $\theta_{\max} = 2\pi/3$ ^{*3}.

Next, we separately standardize the coordinates of the points in the historical map and those in the present map (origin: centroid of all points, mean distance from the centroid: unity) to eliminate the influence of the scale difference between the two maps. We use the following symbols for the standardized points:

$P_{In}(x_{In}, y_{In})$ for P_{Hn} in the input (i.e., historical) map

$P_{On}(x_{On}, y_{On})$ for P_{Pn} in the output (i.e., present) map

($1 \leq n \leq N_P$)

$L_{sIm}(x_{sIm}, y_{sIm})$ for L_{sHm} in the input map

$L_{eIm}(x_{eIm}, y_{eIm})$ for L_{eHm} in the input map

$L_{sOm}(x_{sOm}, y_{sOm})$ for L_{sPm} in the output map

$L_{eOm}(x_{eOm}, y_{eOm})$ for L_{ePm} in the output map

($1 \leq m \leq N_L$)

The position vectors of the centroids of the input and output maps, $\bar{\mathbf{p}}_I$ and $\bar{\mathbf{p}}_O$, are given as follows:

$$\bar{\mathbf{p}}_I = \frac{\sum_{n=1}^{N_P} \mathbf{p}_{Hn} + \sum_{m=1}^{N_L} \{\mathbf{l}_{sHm} D_s(m) + \mathbf{l}_{eHm} D_e(m)\}}{N_P + \sum_{m=1}^{N_L} \{D_s(m) + D_e(m)\}} \quad (6)$$

$$\bar{\mathbf{p}}_O = \frac{\sum_{n=1}^{N_P} \mathbf{p}'_{Pn} + \sum_{m=1}^{N_L} \{\mathbf{l}'_{sPm} D_s(m) + \mathbf{l}'_{ePm} D_e(m)\}}{N_P + \sum_{m=1}^{N_L} \{D_s(m) + D_e(m)\}} \quad (7)$$

^{*2} Another solution can be used as the need arises.

^{*3} The search interval can be varied as the need arises.

where

$$D_s(m) = \begin{cases} 0 & (\text{when } \mathbf{l}_{sHm} = \mathbf{l}_{sHm_0} \text{ or } \mathbf{l}_{sHm} = \mathbf{l}_{eHm_0} \\ & \text{for some } m_0, 1 \leq m_0 < m) \\ 1 & (\text{when } \mathbf{l}_{sHm} \neq \mathbf{l}_{sHm_0} \text{ and } \mathbf{l}_{sHm} \neq \mathbf{l}_{eHm_0} \\ & \text{for any } m_0, 1 \leq m_0 < m) \end{cases} \quad (8)$$

$$D_e(m) = \begin{cases} 0 & (\text{when } \mathbf{l}_{eHm} = \mathbf{l}_{sHm_0} \text{ or } \mathbf{l}_{eHm} = \mathbf{l}_{eHm_0} \\ & \text{for some } m_0, 1 \leq m_0 < m) \\ 1 & (\text{when } \mathbf{l}_{eHm} \neq \mathbf{l}_{sHm_0} \text{ and } \mathbf{l}_{eHm} \neq \mathbf{l}_{eHm_0} \\ & \text{for any } m_0, 1 \leq m_0 < m) \end{cases} \quad (9)$$

$D_s(m)$ and $D_e(m)$ are introduced to remove the endpoints of the control line segments overlapping with any endpoint already used in the calculation^{*4}. By using the above centroid positions, we obtain the standardized position vectors as follows:

$$\begin{aligned} \mathbf{p}_{In} &= [x_{In} \ y_{In}]^T = (\mathbf{p}_{Hn} - \bar{\mathbf{p}}_I) / \bar{d}_I \text{ for } P_{In} \\ \mathbf{p}_{On} &= [x_{On} \ y_{On}]^T = (\mathbf{p}'_{Pn} - \bar{\mathbf{p}}_O) / \bar{d}_O \text{ for } P_{On} \\ \mathbf{l}_{sIm} &= [x_{sIm} \ y_{sIm}]^T = (\mathbf{l}_{sHm} - \bar{\mathbf{p}}_I) / \bar{d}_I \text{ for } L_{sIm} \\ \mathbf{l}_{eIm} &= [x_{eIm} \ y_{eIm}]^T = (\mathbf{l}_{eHm} - \bar{\mathbf{p}}_I) / \bar{d}_I \text{ for } L_{eIm} \\ \mathbf{l}_{sOm} &= [x_{sOm} \ y_{sOm}]^T = (\mathbf{l}'_{sPm} - \bar{\mathbf{p}}_O) / \bar{d}_O \text{ for } L_{sOm} \\ \mathbf{l}_{eOm} &= [x_{eOm} \ y_{eOm}]^T = (\mathbf{l}'_{ePm} - \bar{\mathbf{p}}_O) / \bar{d}_O \text{ for } L_{eOm} \end{aligned} \quad (10)$$

$$\bar{d}_I = \frac{1}{N_P + \sum_{m=1}^{N_L} \{D_s(m) + D_e(m)\}} \left[\sum_{n=1}^{N_P} |\mathbf{p}_{Hn} - \bar{\mathbf{p}}_I| + \sum_{m=1}^{N_L} \{|\mathbf{l}_{sHm} - \bar{\mathbf{p}}_I| D_s(m) + |\mathbf{l}_{eHm} - \bar{\mathbf{p}}_I| D_e(m)\} \right] \quad (11)$$

$$\bar{d}_O = \frac{1}{N_P + \sum_{m=1}^{N_L} \{D_s(m) + D_e(m)\}} \left[\sum_{n=1}^{N_P} |\mathbf{p}'_{Pn} - \bar{\mathbf{p}}_O| + \sum_{m=1}^{N_L} \{|\mathbf{l}'_{sPm} - \bar{\mathbf{p}}_O| D_s(m) + |\mathbf{l}'_{ePm} - \bar{\mathbf{p}}_O| D_e(m)\} \right] \quad (12)$$

The above advance-preparation transformation is similar to the least-squares Euclidean transformation consisting of rotation, translation and scale change [13]. On the other hand, as will be mentioned in Section 3.2, an inverse transformation in which the input and output maps are exchanged is needed in the actual correction process. In the inverse transformation, it is required that the relative positional relationship between the input and output maps is maintained. This relationship is maintained in the inverse transformation of the proposed advance preparation, whereas it is not necessarily maintained in that of the least-squares Euclidean transformation.

2.2 Geometric Correction Based on Vector Field Analysis

This section describes the detail of the geometric correction based on vector field analysis. We first arrange both the input (i.e., historical) and output (i.e., present) maps in a three-dimensional space as shown in **Fig. 1**. The input map is put on the xy plane ($z = 0$), whereas the output map is put on the $z = 1$ plane parallel to the xy plane. In Fig. 1, each of the control points in the input map is connected by a straight line with the corresponding control point in the output map. We give each connected control

^{*4} As will be shown in the example maps in Section 3, a control line segment is often arranged so that its endpoints (or one of its endpoints) coincide with those of other control line segments. To avoid overestimating the weight of the position on which many endpoints overlap, we remove overlapping endpoints in the calculation of the centroid coordinates by introducing $D_s(m)$ and $D_e(m)$.

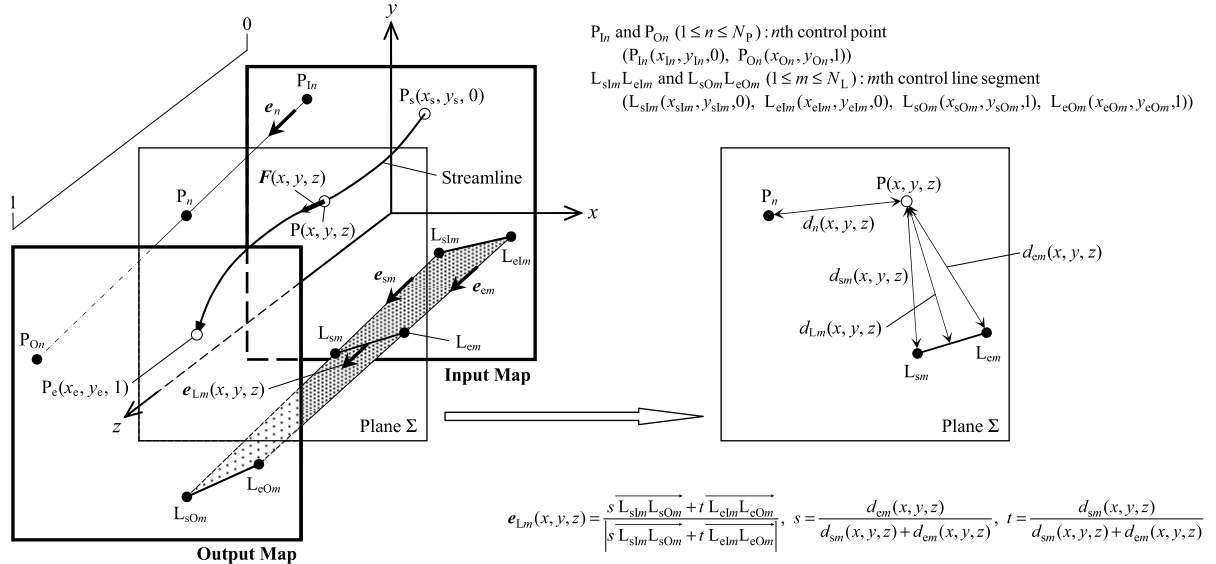


Fig. 1 Concept of vector field analysis.

point pair a unit vector as follows:

$$\begin{aligned} \mathbf{e}_n &= \frac{x_{On} - x_{1n}}{r_n} \mathbf{i} + \frac{y_{On} - y_{1n}}{r_n} \mathbf{j} + \frac{1}{r_n} \mathbf{k} \\ &= e_{nx} \mathbf{i} + e_{ny} \mathbf{j} + e_{nz} \mathbf{k} \end{aligned} \quad (13)$$

$$r_n = \sqrt{(x_{On} - x_{1n})^2 + (y_{On} - y_{1n})^2 + 1^2}$$

where \mathbf{e}_n is the unit vector given to the straight line of the n th control point (i.e., Line $P_{1n}P_{On}$, hereafter the n th CP line) and \mathbf{i} , \mathbf{j} and \mathbf{k} are the fundamental vectors for the x , y and z axes, respectively.

Similarly, each of the endpoints of the control line segments in the input map is connected by a straight line with the corresponding endpoint in the output map as shown in Fig. 1. We give each straight line a unit vector as follows:

$$\begin{aligned} \mathbf{e}_{sm} &= \frac{x_{sOm} - x_{s1m}}{r_{sm}} \mathbf{i} + \frac{y_{sOm} - y_{s1m}}{r_{sm}} \mathbf{j} + \frac{1}{r_{sm}} \mathbf{k} \\ &= e_{smx} \mathbf{i} + e_{smy} \mathbf{j} + e_{smz} \mathbf{k} \end{aligned} \quad (14)$$

$$r_{sm} = \sqrt{(x_{sOm} - x_{s1m})^2 + (y_{sOm} - y_{s1m})^2 + 1^2}$$

and

$$\begin{aligned} \mathbf{e}_{em} &= \frac{x_{eOm} - x_{e1m}}{r_{em}} \mathbf{i} + \frac{y_{eOm} - y_{e1m}}{r_{em}} \mathbf{j} + \frac{1}{r_{em}} \mathbf{k} \\ &= e_{emx} \mathbf{i} + e_{emy} \mathbf{j} + e_{emz} \mathbf{k} \end{aligned} \quad (15)$$

$$r_{em} = \sqrt{(x_{eOm} - x_{e1m})^2 + (y_{eOm} - y_{e1m})^2 + 1^2}$$

where \mathbf{e}_{sm} and \mathbf{e}_{em} are the unit vectors given to the straight lines of the endpoints of the m th control line segment (i.e., Lines $L_{s1m}L_{sOm}$ and $L_{e1m}L_{eOm}$, hereafter the m th CLSs and CLSe lines).

We assume that the vector field $\mathbf{F}(x, y, z)$ shown below exists in the three-dimensional space:

$$\mathbf{F}(x, y, z) = \frac{\sum_{n=1}^{N_p} w(d_n(x, y, z)) \mathbf{e}_n + \sum_{m=1}^{N_l} w(d_{L_m}(x, y, z)) \mathbf{e}_{L_m}(x, y, z)}{\sum_{n=1}^{N_p} w(d_n(x, y, z)) + \sum_{m=1}^{N_l} w(d_{L_m}(x, y, z))} \quad (16)$$

$$w(d) = \frac{1}{d^q}$$

$$d_n(x, y, z) = \sqrt{(x_n(z) - x)^2 + (y_n(z) - y)^2}$$

$$x_n(z) = x_{1n} + a e_{nx}, \quad y_n(z) = y_{1n} + a e_{ny}, \quad a = z / e_{nz}$$

$$d_{L_m}(x, y, z) = \sqrt{\{s x_{sm}(z) + t x_{em}(z) - x\}^2 + \{s y_{sm}(z) + t y_{em}(z) - y\}^2}$$

$$x_{sm}(z) = x_{s1m} + b e_{smx}, \quad y_{sm}(z) = y_{s1m} + b e_{smy}, \quad b = z / e_{smz}$$

$$x_{em}(z) = x_{e1m} + c e_{emx}, \quad y_{em}(z) = y_{e1m} + c e_{emy}, \quad c = z / e_{emz}$$

$$s = \frac{d_{em}(x, y, z)}{d_{sm}(x, y, z) + d_{em}(x, y, z)}$$

$$t = \frac{d_{sm}(x, y, z)}{d_{sm}(x, y, z) + d_{em}(x, y, z)}$$

$$d_{sm}(x, y, z) = \sqrt{(x_{sm}(z) - x)^2 + (y_{sm}(z) - y)^2}$$

$$d_{em}(x, y, z) = \sqrt{(x_{em}(z) - x)^2 + (y_{em}(z) - y)^2}$$

$$\mathbf{e}_{L_m}(x, y, z) = \frac{s \overrightarrow{L_{s1m}L_{sOm}} + t \overrightarrow{L_{e1m}L_{eOm}}}{\left| s \overrightarrow{L_{s1m}L_{sOm}} + t \overrightarrow{L_{e1m}L_{eOm}} \right|}$$

$$\overrightarrow{L_{s1m}L_{sOm}} = (x_{sOm} - x_{s1m}) \mathbf{i} + (y_{sOm} - y_{s1m}) \mathbf{j} + 1 \cdot \mathbf{k}$$

$$\overrightarrow{L_{e1m}L_{eOm}} = (x_{eOm} - x_{e1m}) \mathbf{i} + (y_{eOm} - y_{e1m}) \mathbf{j} + 1 \cdot \mathbf{k}$$

where $d_n(x, y, z)$ is the distance of the point $P(x, y, z)$ (existing at any position in the vector field) from the point $P_n(x_n(z), y_n(z), z)$, i.e., the intersection of the n th CP line with the plane including P (Plane Σ in Fig. 1, parallel to the xy plane), $d_{L_m}(x, y, z)$ is the distance of P from the control line segment on Σ , $L_{sm}L_{em}$ ⁵ ($L_{sm}(x_{sm}(z), y_{sm}(z), z)$ and $L_{em}(x_{em}(z), y_{em}(z), z)$ are the intersections of the m th CLSs and CLSe lines with Σ , respectively), $d_{sm}(x, y, z)$ and $d_{em}(x, y, z)$ are the distances of P from L_{sm} and L_{em} , respectively, $\mathbf{e}_{L_m}(x, y, z)$ is the unit vector given to the m th control line segment, and q is the parameter to adjust the strength of the weight function $w(d)$ (d : distance of P from the point P_n , d_n , or from the line segment $L_{sm}L_{em}$, d_{L_m}). A greater value of q assigns greater influence to the control points or the line segments

⁵ Note that the above distance does not necessarily match that of P from the closest point on $L_{sm}L_{em}$. We adopted the above distance to consider the influence of an entire line segment. In the case that the distance from the closest point is used, the influence of only a single point is considered.

closer to the point P^* .

$F(x, y, z)$ is the weighted mean of e_n s and e_{L_m} s with the inverse distance weight $w(d)$, and becomes smooth everywhere when $q > 1$ [14]. $F(x, y, z)$ has a positive (i.e., non-zero) z -component everywhere because each of the z -components of e_n s and e_{L_m} s, i.e., $1/r_n$ and $1/|\overrightarrow{sL_{sIm}L_{sOm}} + \overrightarrow{tL_{eIm}L_{eOm}}|$, is necessarily positive. As a result, only one streamline of $F(x, y, z)$ passes through any point^{*7}, and each streamline necessarily connects any point in the input map (e.g., $P_s(x_s, y_s, 0)$ in Fig. 1) with only one point in the output map (e.g., $P_e(x_e, y_e, 1)$ in Fig. 1)^{*8}. The region consisting of the intersections of the output-map plane with the streamlines from all the points in the input map (including those other than the control points) becomes the entire area of the corrected input map, and any point in this area is connected with only one point in the input map^{*9}. The above connection can be regarded as a one-to-one onto mapping $h: I \rightarrow O$ (I : set of all points in the input map and O : set of all points in the entire corrected-map area of the output map). When $q > 1$, both h and h^{-1} are not only continuous but also smooth because $F(x, y, z)$ is smooth everywhere. Consequently, h becomes a smooth homeomorphism^{*10}.

On the other hand, consider the case that the point P_s in the input map exists on a control line segment, e.g., the m th control line segment $L_{sIm}L_{eIm}$. We assume that P_s internally divides $L_{sIm}L_{eIm}$ in the ratio $t : s$ ($t = d_s/(d_s + d_e)$, $s = d_e/(d_s + d_e)$, d_s and d_e : distances of P_s from L_{sIm} and L_{eIm} , respectively). In this case, the distance of P_s from the line segment $L_{sIm}L_{eIm}$, d_{L_m} , is zero. Therefore, the streamline starting from P_s becomes a straight line parallel to e_{L_m} , because the inverse distance weight $w(d_{L_m})$ for $L_{sIm}L_{eIm}$ becomes infinite and consequently only the unit vector e_{L_m} contributes to determining the form of the streamline. Since the direction of e_{L_m} is identical to that of $\overrightarrow{sL_{sIm}L_{sOm}} + \overrightarrow{tL_{eIm}L_{eOm}}$, the intersection of the above streamline with the output map, P_e , becomes an internally dividing point of the control line segment $L_{sOm}L_{eOm}$ with the division ratio identical to that of P_s dividing $L_{sIm}L_{eIm}$. This means that the straightness of the control line segment is necessarily maintained in the output map.

As mentioned above, the mapping h simultaneously satisfies Conditions (a) and (b) pointed out in Section 1, i.e., maintains both the property of homeomorphism and the straightness of designated line segments. We adopt this mapping as a point location conversion method for the geometric correction of historical maps. A streamline of $F(x, y, z)$ is obtained by giving a starting

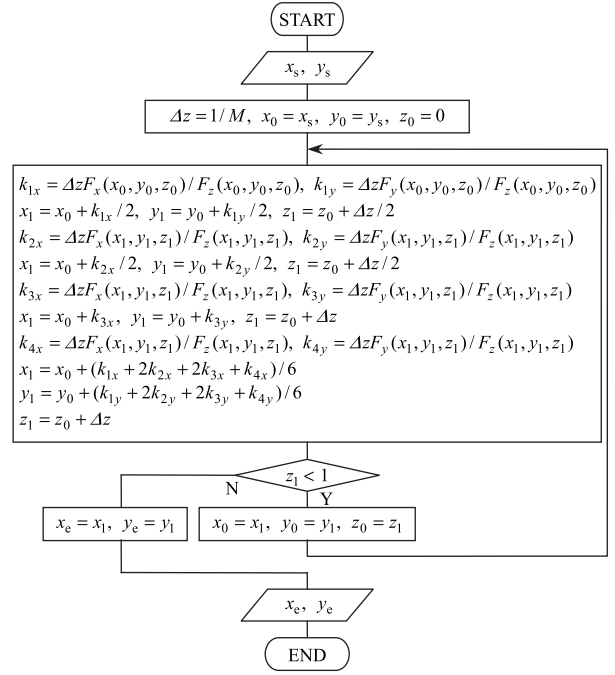


Fig. 2 Algorithm for streamline tracing (Runge-Kutta method, M : division number of the interval $[0, 1]$ in the z axis).

point and solving the equation shown below [8]:

$$\frac{dx}{F_x(x, y, z)} = \frac{dy}{F_y(x, y, z)} = \frac{dz}{F_z(x, y, z)} \quad (17)$$

where $F_x(x, y, z)$, $F_y(x, y, z)$ and $F_z(x, y, z)$ are the x -, y - and z -components of $F(x, y, z)$, respectively. From Eq. (17), two differential equations are derived as follows:

$$\frac{dx}{dz} = \frac{F_x(x, y, z)}{F_z(x, y, z)}, \quad \frac{dy}{dz} = \frac{F_y(x, y, z)}{F_z(x, y, z)} \quad (18)$$

We numerically solve Eq. (18). First, the point location in the input map, $P_s(x_s, y_s, 0)$, is input as a starting point. This point is the point to be converted into that in the output map, and has already been rotated and standardized by the advance-preparation procedure. Next, the algorithm shown in **Fig. 2** (the Runge-Kutta method [15]) is executed. The execution is completed when the streamline reaches the output map, i.e., the $z = 1$ plane. Finally, the x - and y -coordinates at the intersection of the plane with the streamline, x_e and y_e , are output. These coordinates are converted into those of the original (i.e., unrotated and non-standardized) present map as follows:

$$\begin{aligned} P_{Pe} &= [x_{Pe} \quad y_{Pe}]^T \\ &= \begin{bmatrix} \cos(-\theta_0) & -\sin(-\theta_0) \\ \sin(-\theta_0) & \cos(-\theta_0) \end{bmatrix} (\vec{d}_O P_e + \vec{p}_O) \end{aligned} \quad (19)$$

where P_{Pe} is the position vector of the converted point in the original present map, $P_{Pe}(x_{Pe}, y_{Pe})$, and $p_e = [x_e \quad y_e]^T$.

As for the computational complexity of the above algorithm, that of the calculation of $F(x, y, z)$, i.e., Eq. (16), is $O(N_P + N_L)$. On the other hand, the number of loop processing in Fig. 2 depends only on the division number of the interval $[0, 1]$ in the z axis, M . This means that the M value can be given independently of the parameters of the historical and present maps. As a result, the computational complexity of the whole algorithm becomes $O(N_P + N_L)$ (or more simply, $O(N)$ for the data size N).

^{*6} Although the physical dimension of $w(d)$ varies by changing the q value, its influence is eliminated due to the existence of $w(d)$ in the denominator of Eq. (16).

^{*7} For a smooth vector field in which no zero-vector point exists, there is only one streamline passing through any point [8], as already mentioned in Section 1.

^{*8} This is caused because the z -component of F is positive everywhere. This means that streamlines of F never turn into the negative z -direction. Therefore, both the input and output maps are intersected by a streamline only once.

^{*9} This section describes the theoretical background of the proposed method. Therefore, the resolution of both the input and output map is assumed to be infinite and thereby an infinite number of streamlines are considered here. In actual applications, image data with a finite resolution are often used. An approach to solve a problem occurring in the use of finite-resolution image data will be mentioned in Section 3.2.

^{*10} The conditions to be satisfied in a homeomorphism are as follows. (1) h is a one-to-one onto mapping and (2) h and h^{-1} are continuous [10].

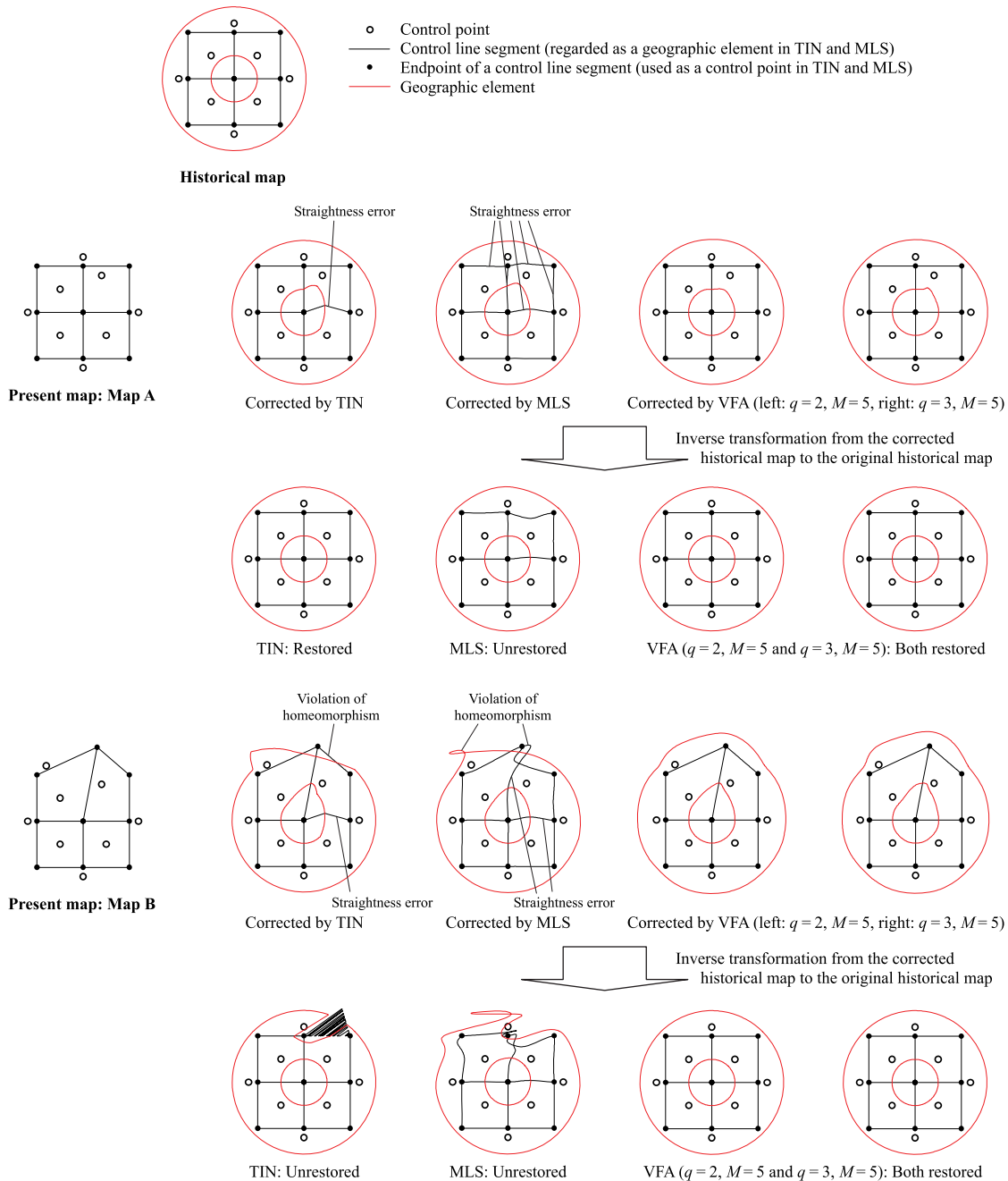


Fig. 3 Geometric correction of the model maps.

3. Results and Discussion

3.1 Overview of Experiments

This section presents the experimental results of the proposed geometric-correction method based on vector field analysis (VFA). As already mentioned in Section 1, we compare the obtained results with those obtained by TIN and MLS. In TIN, the Delaunay triangulation [16] is used to construct a triangulated irregular network (no additional procedure modifying the structure of the network is used), whereas the affine transformation is used for local coordinate conversion in each triangle area [4].

First, simple artificial mapping models are used to compare the performance of VFA with those of TIN and MLS. Next, the historical map of Akita City, Japan, is used to evaluate the charac-

teristics shown in the geometric correction of an actual historical map.

3.2 Geometric Correction of Simple Mapping Models

Figure 3 shows the results of geometric correction for the simple mapping models. The historical map consists of 8 control points, 12 control line segments and 2 circles, and is converted into two present maps: Maps A and B. In the experiments, the points existing on the 12 control line segments in the historical map (64 points for each control line segment) and those on the 2 circles (360 points for each circle) are converted into those in the 2 present maps. In addition, the inverse transformation, in which the corrected historical maps are used as input maps and the orig-

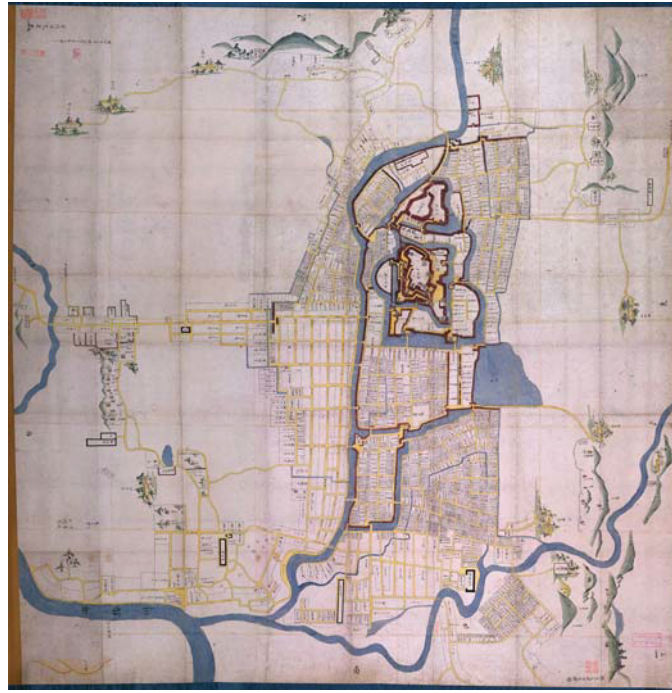


Fig. 4 Historical map *Ushū Kubota Ōezu* (representing the situation of the Kubota district (current Akita City, Akita Prefecture, Japan) in 1828) [17].

inal historical map is used as an output map, is performed^{*11}. In the experiments in which TIN or MLS is used, the endpoints of the control line segments are used as control points (overlapping ones are removed). As for the experiments of VFA, the results of 2 cases in which the value of q in Eq. (16) is changed ($q = 2$ or 3) are shown ($M = 5$ in both cases. The appropriateness of this M value will be demonstrated in the latter part of this section.).

In the cases of Map A, the corrected historical maps given by TIN and MLS show errors in the straightness maintenance of the control line segments. On the other hand, the straightness of all the control line segments is maintained in both the 2 corrected historical maps given by VFA. As for the inverse transformation, the original historical map is completely restored in TIN and the 2 cases of VFA, whereas restoration is failed in the case of MLS.

In the cases of Map B in which the configuration of the control points and line segments is more highly deformed than Map A, the corrected historical maps given by TIN and MLS show not only errors in straightness maintenance but also the violation of homeomorphism. On the other hand, no error is seen in both the 2 cases of VFA. As for the inverse transformation, the restoration of the original historical map is succeeded in both the 2 cases of VFA, whereas it is failed in TIN and MLS.

The above results show the advantage of the proposed VFA method. In particular, it should be noted that VFA is more robust against a highly deformed control-point configuration than the other two methods. This property is maintained through the change of the parameter q . As shown in Fig. 3, the shapes of the geographic elements (i.e., 2 circles) are slightly changed by changing the q value. This means that users can adjust the shapes of geographic elements to a certain extent by changing the q

^{*11} In the inverse transformation of TIN, the structure of the triangulated irregular network obtained in the forward transformation is kept.

Table 1 Errors of the locations of the geographic elements (2 circles in Map B) restored by the inverse transformation performed by VFA.

		$M = 2$	$M = 3$	$M = 5$	$M = 10$
$q = 2$	Max	1.57×10^{-4}	2.45×10^{-5}	2.03×10^{-6}	6.49×10^{-8}
	Mean	4.11×10^{-6}	5.43×10^{-7}	4.40×10^{-8}	1.40×10^{-9}
$q = 3$	Max	6.40×10^{-4}	1.02×10^{-4}	8.21×10^{-6}	2.68×10^{-7}
	Mean	2.44×10^{-5}	3.44×10^{-6}	2.91×10^{-7}	9.61×10^{-9}

value.

As for the restoration of the original historical map in the inverse transformation, only VFA succeeded in all the cases. As will be shown in the next section, the geometric correction of a historical map is often performed using the image data of the map. In such cases, a blank (or multiple blanks) appears inside the image data of the corrected historical map obtained by the forward transformation, due to a partial stretch caused by a highly localized deformation of the control-point configuration. By using the procedure of the inverse transformation, we can identify the historical-map locations corresponding to all the pixels in the image data of the present map. As a result, the appearance of a blank part inside the corrected historical map can be avoided. In the above identification process, it is desirable that the correspondence between the locations of the historical map and those of the present map is uniquely determined through both the forward and inverse transformations. VFA, which restores the original historical map in all the cases of the inverse transformation, realizes the above unique correspondence. TIN also realizes the unique correspondence only in the case that no violation of homeomorphism occurs.

To investigate the influence of the variation of the M value (i.e., the division number of the z axis in the numerical streamline tracing) on the accuracy of the VFA geometric correction, we calculate the errors of the locations of the geographic elements in

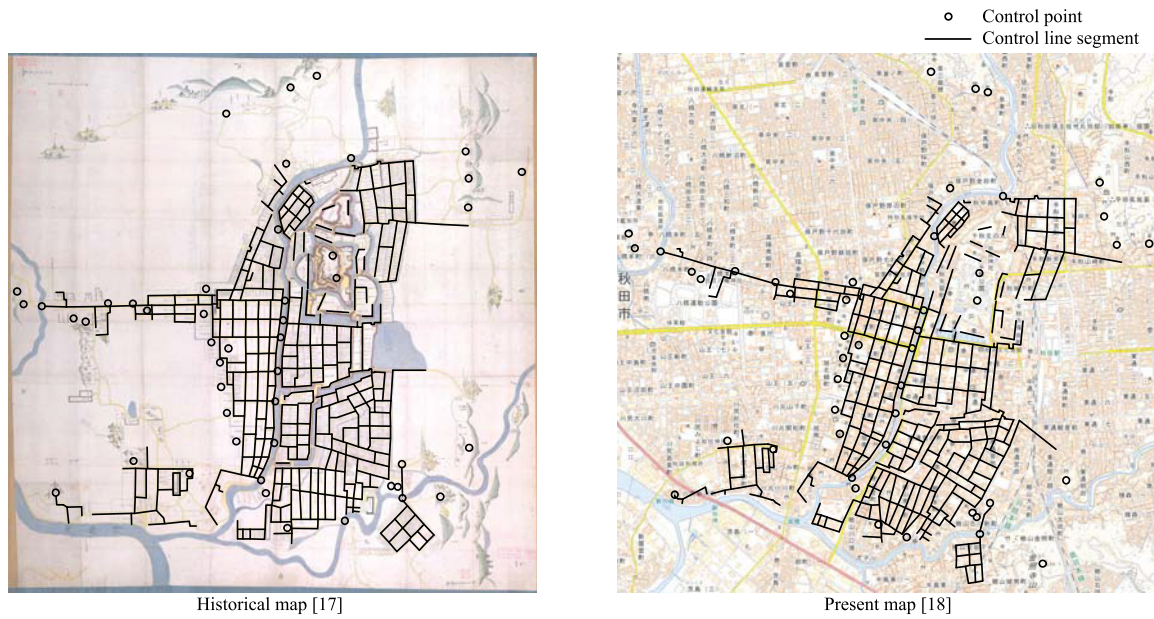


Fig. 5 Control points and control line segments used in geometric correction.

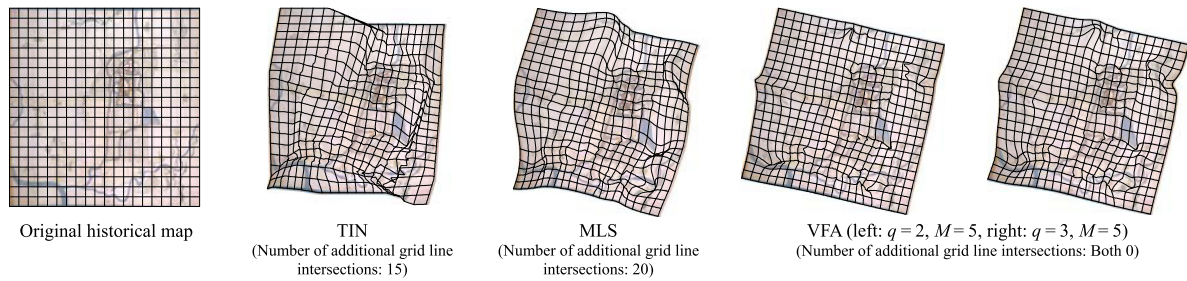


Fig. 6 Evaluation of homeomorphism by counting the number of grid line intersections.

the historical map restored in the inverse transformation. Table 1 shows the errors of the locations of the circles restored by the inverse transformation. Specifically, error values are calculated at every point comprising the 2 circles in Map B as follows:

$$e_k = \frac{\sqrt{(x_{rk} - x_{ok})^2 + (y_{rk} - y_{ok})^2}}{r_0} \quad (20)$$

where x_{rk} and y_{rk} are the coordinates of the k th restored point ($1 \leq k \leq 720$), x_{ok} and y_{ok} are those of the k th original point and r_0 is the radius of the outer circle. As shown in the table, the error value can be kept within less than 10^{-5} when $M \geq 5$. This means that at least five significant digits are guaranteed when $M \geq 5$ ^{*12}. In the next section in which the geometric correction of an actual historical map is performed, we set $M = 5$ because positions in the historical map used in the next section are represented by four-significant-digit pixel numbers.

3.3 Geometric Correction of an Actual Historical Map

As mentioned above, this section presents the experimental results of the geometric correction of an actual historical map. Figure 4 shows the historical map used in the experiments. This is the historical map *Ushū Kubota Ōezu* representing the situation of the Kubota district (current Akita City, Akita Prefecture,

^{*12} In the case that the degree of deformation is much higher than the cases of Fig. 3, a larger M value may be needed. It can be confirmed whether the selected M value is appropriate or not by checking the inverse-transformation accuracy.

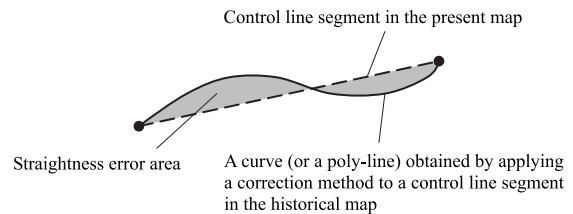


Fig. 7 Evaluation of line-segment straightness by using the straightness error area.

Japan) in 1828 [17]^{*13}. The size of the image data of the map is as follows: width: 2,006 [px] and height: 2,048 [px].

Figure 5 shows the configuration of the control points and control line segments in the historical map and that in the present map^{*14}. 47 control points (existing temples, shrines, bridges, etc.) and 675 control line segments (existing roads, moats, etc.) are used^{*15}. The coordinates of the control points and the end-

^{*13} The image data of the historical map was downloaded from the web site of Akita Prefectural Library Digital Archive [17]. This map originally puts east on top. However, the map used in this paper, i.e., the map shown in Fig. 4, is rotated 90 degrees clockwise to put north on top in accordance with the current conventions in surveying. The present map is further rotated by the direction optimization procedure mentioned in Section 2.1.

^{*14} The image data of the present map was downloaded from the web site of Geospatial Information Authority of Japan [18].

^{*15} Since the purpose of this paper is to solve technical problems in the geometric correction of historical maps, we do not historically validate the selection of the control points and control line segments shown in Fig. 5.

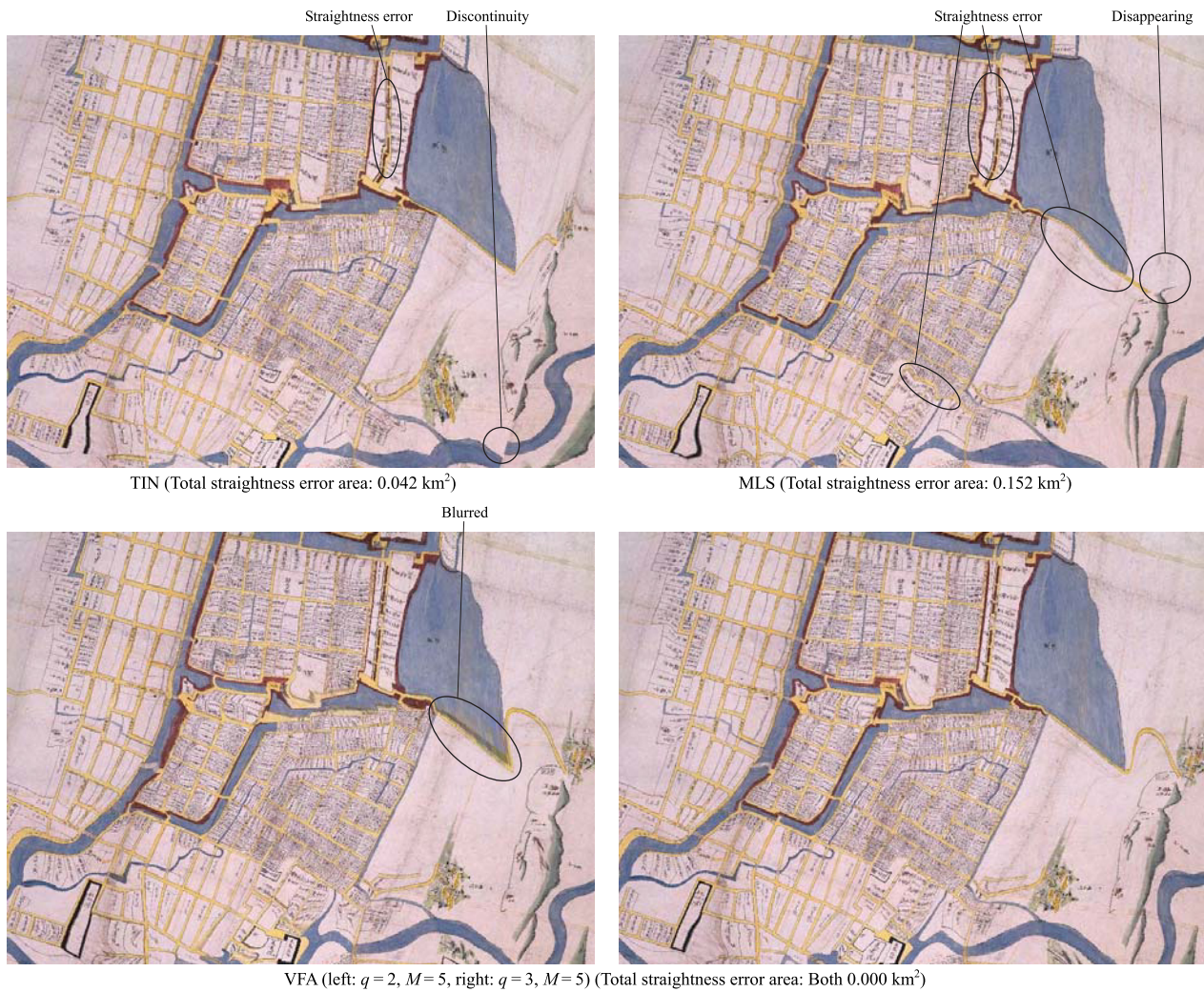


Fig. 8 Geometric correction of the historical map *Ushū Kubota Ōezu*.

points of the control line segments in the present map are determined by converting the values of latitude and longitude, obtained from Google Map [19], into the coordinates on the plane of the Japanese Plane Rectangular Coordinate System X [11], [20].

The historical map of Fig. 4 is corrected by TIN, MLS and VFA. In the experiments of TIN and MLS, the endpoints of the control line segments are used as the control points (overlapping ones are removed). On the other hand, the procedure of inverse transformation is adopted in the experiments of TIN and VFA to avoid the appearance of a blank part inside the image data of the corrected historical map. As for the experiment of MLS, we use the procedure of forward transformation instead of inverse transformation, due to the fact that MLS cannot realize the unique correspondence between the locations of the historical map and those of the present map, as already mentioned in Section 3.2. In this case, the information on the blank parts inside the corrected historical map is given by nearest neighbor interpolation [21].

To evaluate whether the correction process is a homeomorphism or not, we draw a grid on the historical map as shown in the leftmost map of Fig. 6^{*16}. When the correction process is

^{*16} In TIN and VFA, only the grid lines are converted by the forward-transformation procedure, because their locations in the present map cannot be known in advance.

a homeomorphism, no additional intersection between the grid lines appears in the corrected historical map. In the cases of TIN and MLS shown in Fig. 6, both the corrected historical maps obtained by these methods give multiple additional intersections (TIN: 15 and MLS: 20), whereas both the two corrected historical maps obtained by VFA give no additional intersection. In other words, only VFA can maintain the property of homeomorphism for the historical map of Fig. 4.

On the other hand, to evaluate whether the straightness of the control line segments is maintained or not, we introduce the concept of the straightness error area shown in Fig. 7. The straightness error area is an area of the region between the original control line segment in the present map and a curve (or a poly-line) obtained by applying a correction method to the corresponding control line segment in the historical map. When the straightness is maintained, the value of the total straightness error area becomes zero.

In the cases of TIN and MLS shown in the upper part of Fig. 8, the corrected historical maps show errors in the straightness maintenance of the control line segments. The total straightness error areas are 0.042 km² for TIN and 0.152 km² for MLS, i.e., non-zero values. In addition, undesirable phenomena such as the discontinuity of a river and the disappearance of a geographic ele-

ment, caused by the violation of homeomorphism, are seen in the cases of TIN and MLS. As for the cases of VFA shown in the lower part of Fig. 8, on the other hand, the total straightness error area is zero in both the cases. This means that the straightness is maintained in both the corrected historical maps given by VFA. However, a blurred part is seen in the $q = 2$ case. The blurring is suppressed in the $q = 3$ case. This suggests the possibility that inappropriate phenomena that appeared in a certain condition are eliminated by adjusting a user parameter such as the q value.

3.4 Discussion

In both the case of the simple mapping models and that of the historical map *Ushū Kubota Ōezu*, the proposed VFA method showed more excellent characteristics than those of TIN and MLS in maintaining both the property of homeomorphism and the straightness of designated line segments. In addition, it was also shown that only VFA gave a unique correspondence between the locations of the historical map and those of the present map through the forward and inverse transformation in every case. This property provides advantages not only in avoiding the appearance of a blank part inside the image data of the corrected historical map, but also in examining the links between the geographic situation in a particular age and that in the present day in detail.

On the other hand, VFA has a disadvantage in calculation time. The calculation times for the 1,003-pixel-width 1,024-pixel-height part in *Ushū Kubota Ōezu* are as follows: TIN: 966 [s], MLS: 1,498 [s] and VFA ($q = 2$, $M = 5$): 46,583 [s] (i.e., over 12 hours) (CPU: Intel Core i3-350M). To resolve this issue, the introduction of an additional effective technique, e.g., a parallel computing technique, etc. is required. Fortunately, it is possible to apply a parallel computing technique to VFA, because streamline tracing for each pixel in the image data of the present map is performed independently of other pixels.

4. Conclusion

The main contribution of this paper is that the two major conditions required for the geometric correction of historical maps (maintaining both the property of homeomorphism and the straightness of designated line segments) are simultaneously satisfied by the proposed VFA method. The experimental results obtained by VFA show more excellent characteristics than those obtained by the other conventional methods. This paper also suggests the adjustability of VFA to obtain geographic elements with a more preferable state, e.g., a more preferable shape with no blurred part. On the other hand, the disadvantage that VFA takes a very long calculation time is also pointed out. Additional research is required to resolve this issue.

Acknowledgments This study was supported by JSPS Grants-in-Aid for Scientific Research (KAKENHI) Grant Number JP18K11981.

References

- [1] Fuse, T., Shimizu, E. and Morichi, S.: A Study on Geometric Correction of Historical Maps, *International Archives of Photogrammetry and Remote Sensing*, Vol.32, No.5, pp.543–548 (1998).
- [2] Cajthaml, J.: Methods of Georeferencing Old Maps on the Example of Czech Early Maps, *Proc. 25th International Cartographic Conference*, CO-314 (2011).
- [3] Herrault, P.A., Sheeren, D., Fauvel, M., Monteil, C. and Paegelow, M.: A Comparative Study of Geometric Transformation Models for the Historical “Map of France” Registration, *Geographia Technica*, No.1, pp.34–46 (2013).
- [4] Dai Prà, E. and Mastrorunzio, M.: Rectify the River, Rectify the Map. Geometry and Geovisualization of Adige River Hydro-Topographic Historical Maps, *e-Perimetron*, Vol.9, No.3, pp.113–128 (2014).
- [5] Ullah, R. and Kraak, M.-J.: An Alternative Method to Constructing Time Cartograms for the Visual Representation of Scheduled Movement Data, *Journal of Maps*, Vol.11, No.4, pp.674–687 (2015).
- [6] Kitamoto, A. and Nishimura, Y.: Geometric Correction of Measured Historical Maps with a Pixel-oriented and Geobrowser-friendly Framework, *Proc. 22nd CIPA Symposium* (2009).
- [7] Shimizu, E. and Fuse, T.: Rubber-Sheeting of Historical Maps in GIS and Its Application to Landscape Visualization of Old-time Cities: Focusing on Tokyo of the Past, *Proc. 8th Intl. Conf. on Computers in Urban Planning and Urban Management*, 11A-3 (2003).
- [8] McLeod, Jr., E.B.: *Introduction to Fluid Dynamics*, Dover Publications, Inc. (2016).
- [9] Miura, T. and Tajima, K.: Point Location Conversion in Distance Cartogram Construction Based on Vector Field Analysis, *Journal of Information Processing*, Vol.28, pp.711–714 (2020).
- [10] Zomorodian, A.J.: *Topology for Computing*, Cambridge University Press (2005).
- [11] Okazawa, H., Kubodera, T., Sasada, K., Tasumi, M., Hosokawa, Y., Matsuo, E. and Mihara, M.: *Newer Surveying: Fundamentals and Applications with Newest Technology*, Corona Publishing Co., Ltd. (2014) (in Japanese).
- [12] Miller, R.E.: *Optimization*, John Wiley & Sons, Inc. (2000).
- [13] Waterman, S. and Gordon, D.: A Quantitative-comparative Approach to Analysis of Distortion in Mental Maps, *Professional Geographer*, Vol.36, No.3, pp.326–337 (1984).
- [14] Shepard, D.: A Two-dimensional Interpolation Function for Irregularly-spaced Data, *Proc. 1968 23rd ACM National Conference*, pp.517–524 (1968).
- [15] Sewell, G.: *The Numerical Solutions of Ordinary and Partial Differential Equations*, Academic Press, Inc. (1988).
- [16] Kang, I.-S., Kim, T.-W., and Li, K.-J.: A Spatial Data Mining Method by Delaunay Triangulation, *Proc. 5th ACM International Workshop on Advances in Geographic Information Systems (GIS 97)*, pp.35–39 (1997).
- [17] Akita Prefectural Library Digital Archive, available from (<https://da.apl.pref.akita.jp/lib/item/00010001/ref-1-1356>).
- [18] Geospatial Information Authority of Japan, available from (<https://maps.gsi.go.jp/help/intro/>).
- [19] Google Map, available from (<https://www.google.co.jp/maps/>).
- [20] Kawase, K.: Concise Derivation of Extensive Coordinate Conversion Formulae in the Gauss-Krüger Projection, *Bulletin of the Geospatial Information Authority of Japan*, Vol.60, pp.1–6 (2013).
- [21] Han, D.: Comparison of Commonly Used Image Interpolation Methods, *Proc. 2nd International Conference on Computer Science and Electronics Engineering (ICCSEE 2013)*, pp.1556–1559 (2013).



Takeshi Miura received his D.Eng. degree in electrical engineering from Hokkaido University in 1998. He is currently an associate professor in the Department of Electrical-Electronic-Computer Engineering, Graduate School of Engineering Science, Akita University.



Katsubumi Tajima received his D.Eng. degree in electrical engineering from Tohoku University in 1998. He is a professor in the Cooperative Major in Life Cycle Design Engineering, Graduate School of Engineering Science, Akita University.